A&A 569, A64 (2014)
DOI: 10.1051/0004-6361/201423911

Astronomy & Astrophysics

MASSIV: Mass Assembly Survey with SINFONI in VVDS

VI. Metallicity-related fundamental relations in star-forming galaxies at $1 < z < 2$⋆,⋆⋆

C. Divoy[1,2], T. Contini[1,2], E. Pérez-Montero[3], J. Queyrel[1,2], B. Epinat[4], C. López-Sanjuan[5], D. Vergani[6], J. Moultaka[1,2], P. Amram[4], B. Garilli[7], M. Kissler-Patig[8], O. Le Fèvre[4], L. Paioro[7], L. A. M. Tasca[4], L. Tresse[4], and V. Perret[4]

[1] Institut de Recherche en Astrophysique et Planétologie (IRAP), CNRS, 14 avenue Édouard Belin, 31400 Toulouse, France
e-mail: cdivoy@irap.omp.eu
[2] IRAP, Université de Toulouse, UPS-OMP, 31028 Toulouse, France
[3] Instituto de Astrofísica de Andalucía – CSIC Apdo. 3004, 18080 Granada, Spain
[4] Aix Marseille Université, CNRS, LAM (Laboratoire d'Astrophysique de Marseille) UMR 7326, 13388 Marseille, France
[5] Centro de Estudios de Física del Cosmos de Aragón, Plaza San Juan 1, planta 2, 44001 Teruel, Spain
[6] INAF-IASFBO, via P. Gobetti 101, 40129 Bologna, Italy
[7] IASF-INAF, via Bassini 15, 20133 Milano, Italy
[8] Gemini Observatory, 670 N. A'ohoku Place, Hilo, Hawaii 96720, USA

Received 31 March 2014 / Accepted 18 June 2014

ABSTRACT

Aims. The MASSIV (Mass Assembly Survey with SINFONI in VVDS) project aims at finding constraints on the different processes involved in galaxy evolution. This study proposes to improve understanding of the galaxy mass assembly through chemical evolution using metallicity as a tracer of the star formation and interaction history.
Methods. We analysed the full sample of MASSIV galaxies for which a metallicity estimate has been possible, the 48 star-forming galaxies at $z \sim 0.9-1.8$, and computed the integrated values of some of the fundamental parameters, such as stellar mass, metallicity, and star formation rate (SFR). The sample of star-forming galaxies at similar redshifts from *z*COSMOS was also combined with the MASSIV sample. We studied the cosmic evolution of the mass-metallicty relation, together with the effect of close environment and galaxy kinematics on this relation. We then focussed on the so-called fundamental metallicity relation and other relations between stellar mass, SFR, and metallicity. We investigated whether these relations are really fundamental, i.e. if they do not evolve with redshift.
Results. The MASSIV galaxies follow the expected mass-metallicity relation for their median redshift. We find, however, a significant difference between isolated and interacting galaxies as found for local galaxies: interacting galaxies tend to have a lower metallicity. The study of the relation between stellar mass, SFR, and metallicity gives such large scattering for our sample, even combined with *z*COSMOS, that it is difficult to confirm any fundamental relation.

Key words. galaxies: abundances – galaxies: evolution – galaxies: fundamental parameters – galaxies: high-redshift

1. Introduction

The current paradigm for galaxy formation is the so-called hierarchical model. It explains the formation of small galaxies at the earliest epochs, mainly by gas accretion in dark matter haloes. Later on in the history of the Universe, these small galaxies merged to produce larger galaxies. During these processes the interstellar medium (ISM) underwent multiple mixings, inducing strong variations in the chemical abundances of galaxies. The abundance of metals in the ISM, defined as the metallicity (Z), is thus a marker of the galaxy star formation history and of the various gas flows (accretion and outflows) that could happen during its life. The metal enrichment of the ISM is due to stellar evolution but is also a consequence of galaxy interactions and/or interplay with the surrounding intergalactic medium. Indeed, both inflows of pristine gas toward the centre of the galaxy and outflows of metal-rich gas due to supernovae-driven galactic winds reduce the nuclear metallicity of galaxies. Metallicity is therefore a fundamental parameter to follow in cosmic time for understanding the formation and evolution of galaxies.

Simulations based on the hierarchical model that includes chemical evolution and feedback processes (Moster et al. 2012; Calura et al. 2012; Stinson et al. 2013) can roughly reproduce observations, but new and more accurate datasets are needed to constrain the free parameters of these simulations, such as the feedback efficiency and accretion rate. For instance, Michel-Dansac et al. (2008) performed simulations to constrain the role of galaxy interactions in the variation of the metallicity. They find that interacting galaxies with low(high) masses have

⋆ This work is based on observations collected at the European Southern Observatory (ESO) Very Large Telescope, Paranal, Chile, as part of the Programs 179.A-0823, 78.A-0177, and 75.A-0318. This work also benefits from data products produced at TERAPIX and the Canadian Astronomy Data Centre as part of the Canada-France-Hawaii Telescope Legacy Survey, a collaborative project of NRC and the CNRS.
⋆⋆ Table 1 is available in electronic form at http://www.aanda.org

higher(lower) metallicities than their isolated counterparts that follow the well-known mass-metallicity relation. During minor mergers the metallicity of the lighter component increases between the start of the interaction and the coalescence, but for a major merger the metallicity of the heavier component increases.

Ever since the seventies, it has been known that there is a link between galaxy luminosity and metallicity. Lequeux et al. (1979) give a relation between these parameters for galaxies in the local universe. Nevertheless, the luminosity is too sensitive to the star formation rate (SFR) and extinction, so subsequent studies introduced a more fundamental parameter: the stellar mass. Large surveys of local galaxies, such as 2dF and SDSS, have been used to study and confirm the relation between stellar mass and metallicity (Lamareille et al. 2004; Tremonti et al. 2004), also called MZR. For instance, Tremonti et al. (2004) established the relation between stellar mass and metallicity for a sample of more than 50 000 local galaxies from the SDSS. The origin of this relation is not yet understood well. We know theoretically that stellar evolution ends with the ejection of metals that enrich the ISM with time and that stellar mass also increases with time mainly by merger processes. As predicted by theory, numerous studies based on distant galaxies (e.g. Erb et al. 2006; Lamareille et al. 2006, 2009; Maiolino et al. 2008; Mannucci et al. 2009; Pérez-Montero et al. 2009, 2013) show that metallicity decreases with redshift up to $z \sim 4$. However, the role of inflows and outflows is not well constrained. Each process is theoretically understood well but their scale factors and their dependence on time are not well defined. For instance, at high redshift, gas inflows are needed to reproduce unusual metallicity gradients in galaxies (e.g. Cresci et al. 2010; Queyrel et al. 2012), but we do not know yet if these gas inflows are mainly due to cold flows or are induced by galaxy interactions. At this point, another parameter seems to play a role in galaxy evolution: the SFR. Mannucci et al. (2010) proposed a relation between mass, metallicity and SFR, called the fundamental metallicity relation (FMR). Independently, Lara-López et al. (2010) have found a fundamental plane in the space defined by these three parameters. The evolution with redshift of these relations is not yet known well and is quite controversial. On one hand, there are studies (e.g. Cresci et al. 2012) finding a non-evolving FMR, and on the other hand, other studies find a MZR evolving with redshift even when they remove the dependence on the SFR (e.g. Pérez-Montero et al. 2013).

In this paper, we use the MASSIV sample (Contini et al. 2012) to investigate the MZR and the FMR in the redshift range $0.9 < z < 1.8$. MASSIV is representative of the star-forming galaxy population at these redshifts, corresponding to a critical cosmic period for galaxy evolution when galaxies change rapidly. The aim of this study is to contribute to our understanding of the physical processes involved in the early stages of galaxy evolution. First results on the MZR, metallicity gradients, and fundamental relations between mass, velocity, and size, which are all based on the so-called "first epoch" MASSIV sample, have been published in Queyrel et al. (2009, 2012), and Vergani et al. (2012), respectively.

This paper is organized as follows. In Sect. 2, we present the galaxy sample obtained from the MASSIV survey and say how we extract Hα and [N II]λ6584 fluxes to compute the SFR and the metallicity of galaxies. In Sect. 3, we investigate the MZR for our sample and its relation with various parameters, such as the redshift, the galaxy kinematics, and their close environment. In Sect. 4 we present an analysis of the relations between stellar mass, metallicity, and SFR for the MASSIV galaxies. In Sect. 5 we discuss the agreement of our results with previous studies.

Throughout the paper, we assume a ΛCDM cosmology with $\Omega_m = 0.3$, $\Omega_\Lambda = 0.7$, and $H_0 = 70\ \mathrm{km\,s^{-1}\,Mpc^{-1}}$.

2. Dataset

2.1. The MASSIV sample

For this analysis we use the full MASSIV (Mass Assembly Survey with SINFONI in VVDS) sample of 83 star-forming galaxies, which is fully described in Contini et al. (2012). Hereafter, we call the 50 galaxies first observed and published in Epinat et al. (2012) the "first epoch" sample, and the "second epoch" sample the last 33 galaxies. These galaxies have been selected in the VVDS (VIMOS VLT Deep Survey (Le Fèvre et al. 2013)) sample to be representative of the population of star-forming galaxies at high redshifts ($z \sim 0.9-1.8$). The selection of galaxies up to redshift $z \sim 1.5$ was based on the intensity and equivalent width of the [O II]λ3727 emission line measured on VIMOS spectra (e.g. Franzetti et al. 2007; Vergani et al. 2008; Lamareille et al. 2009). The selection of galaxies at higher redshift was based mainly on their rest-frame ultraviolet continuum and/or massive stars absorption lines. These star formation criteria ensure that the rest-frame optical emission lines Hα and [N II]λ6584 or, in a few cases, [O III]λ5007 are bright enough to be observed with the Integral Field Unit SINFONI in the near-infrared J (sources at $z < 1.1$) and H (sources at $z > 1.2$) bands. As shown in Contini et al. (2012), the final MASSIV sample provides a good representation of "normal" star-forming galaxies at $0.9 < z < 1.8$ in the stellar mass regime $M_* = 10^9-10^{11}\ M_\odot$, with a median $SFR \sim 30\ M_\odot\ \mathrm{yr}^{-1}$ and a detection threshold of $\sim 5\ M_\odot\ \mathrm{yr}^{-1}$.

SINFONI observations were performed between April 2007 and January 2011. Most (85%) of the targeted galaxies were observed in a seeing-limited mode (with a spatial sampling of 0.125″/pixel). Eleven galaxies were acquired with adaptive optics (AO) assisted with a laser guide star (seven with 0.05″ and four with 0.125″/pixel spatial sampling).

The data reduction was performed with the ESO SINFONI pipeline (version 2.0.0), using the standard master calibration files provided by ESO. The absolute astrometry for the SINFONI data cubes was derived from nearby bright stars also used for point spread function measurements. Custom IDL and Python scripts were used to flux calibrate, align, and combine all the individual exposures. For each galaxy, a non-sky-subtracted cube was also created, mainly to estimate the effective spectral resolution. For more details on data reduction, we refer to Epinat et al. (2012).

2.2. Line measurement

2.2.1. Extraction of 1D spectra

Spectra were extracted from both flux-calibrated and counts datacubes on apertures corresponding to a signal-to-noise ratio (S/N) on the Hα line larger than 2 and to spaxels where the line is narrower than the spectral resolution. S/N maps were obtained using a 2×2 spaxel Gaussian smoothing as described in Epinat et al. (2012). Isolated extra-spaxels with a $S/N > 2$ were removed based on a visual inspection. Spectra of all the spaxels belonging to the aperture were shifted in wavelength according to their corresponding Hα line position, and then summed to obtain the final 1D integrated spectrum.This shift enables a spectrum with narrower lines, which is better fitted by a Gaussian function than in the case where the velocity gradient is not removed. This

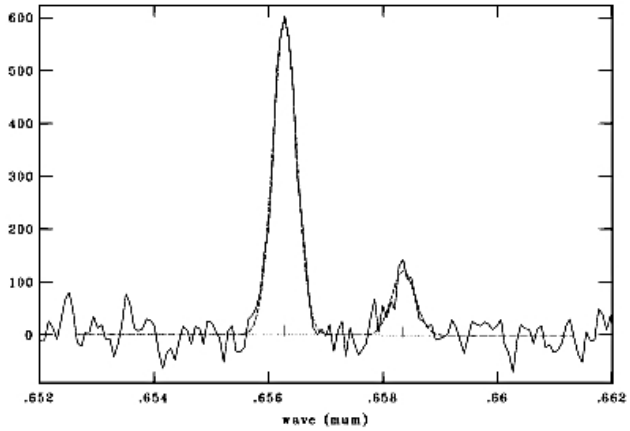

Fig. 1. One example of the measurement of Hα and [N II]λ6584 emission lines with SPLOT task of IRAF. The spectrum and the fitted Gaussians are shown with solid and dotted lines respectively. Intensity units are expressed in number counts and rest-frame wavelength units in μm.

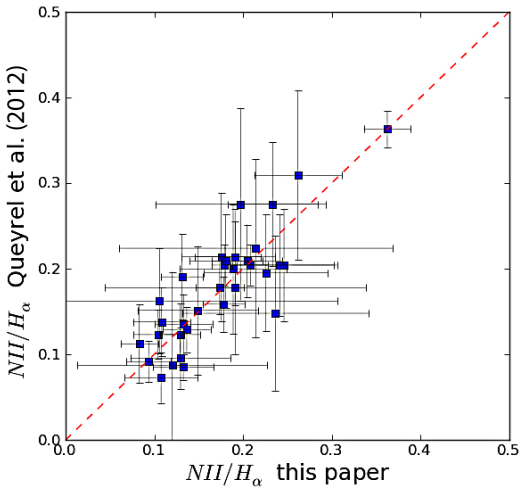

Fig. 2. Comparison between the [N II]/Hα flux ratios measured in this paper and those published in Queyrel et al. (2012). The agreement is good when error bars, coming essentially from measurement uncertainties, are taken into account ($\chi^2 = 0.648$).

procedure also increases the S/N in the final integrated spectrum and therefore the accuracy of line measurements.

2.2.2. Procedure to measure emission lines

To compute metallicities, we need to measure the flux of Hα and [N II]λ6584 emission lines. To do so we use the task SPLOT of IRAF to fit Gaussian functions on the different lines of the 1D spectrum of each galaxy. We obtain the flux and associated errors with the deblending mode of this task SPLOT with the constraint that the FWHM of the Hα and [N II]λ6584 lines are the same (see Fig.1).

For some galaxies the lines were not measurable for two main reasons: either the intensity of the lines is too low to be measured, so there is no detection for these lines, or there are some strong sky line residuals at the same wavelength as the expected lines. For the second epoch sample, there are seven galaxies with no detection of the [N II]λ6584 emission line, VVDS020258016, 910154631, 910184233, 910187744, 910232719, 910296626, 910300117, and six galaxies with strong sky line residuals at the wavelength of Hα or [N II]λ6584 emission lines: VVDS910159867, 910177382, 910191357, 910195040, 910274060, 910377628. Similar situation occurred for the first epoch sample and have been explained in Queyrel et al. (2012).

2.3. Metallicity

We were able to derive the integrated metallicity for 48 galaxies of the sample. Metallicity is computed using the flux ratio between Hα and [N II]λ6584 emission lines, the so-called N2 parameter. This parameter has a monotonic linear relation with oxygen abundance up to oversolar values and it has the advantage of having almost no dependence with reddening or flux calibration. Although N2 is also related to ionization parameter and the nitrogen-to-oxygen abundance ratio, the empirical calibration proposed by Pérez-Montero & Contini (2009), based on objects with a direct determination of the electron temperature, leads to metallicities with an uncertainty around 0.3 dex. For the identified interacting galaxy pairs (see López-Sanjuan et al. 2013), the spectrum of the main component has been extracted and used to compute the metallicity. Depending on the calibration used, the derived metallicities can change significantly. We use the relation given by Kewley & Ellison (2008) and Queyrel et al. (2009) to convert metallicities computed with the Pérez-Montero & Contini (2009) calibration to metallicities using the Tremonti et al. (2004) calibration. This relation is

$$y = -0.217468x^3 + 5.80493x^2 - 50.2318x + 149.836 \quad (1)$$

where x or $Z_{\rm PMC09}$ is the metallicity in Pérez-Montero & Contini (2009) calibration and y or Z_{T04} metallicity in Tremonti et al. (2004) calibration. For each galaxy, Table 1 contains the galaxy VVDS identification number, the redshift as derived from the SINFONI data using the position of the Hα line, the flux of the Hα line, the flux ratio between [N II]λ6584 and Hα lines, the metallicity computed with the Pérez-Montero & Contini (2009) calibration, and the recalibration of this metallicity to Tremonti et al. (2004) calibration.

The Hα flux, the flux ratio [N II]/Hα, and the metallicity for 34 galaxies of the first epoch sample of MASSIV have already been published in Queyrel et al. (2012). For the sake of homogeneity, we derive these quantities again for the full MASSIV sample using the same procedure as Queyrel et al. (2012). Figure 2 shows the comparison of previous and new measurements for the [N II]/Hα flux ratio. Measurements are consistent with each other when taking the uncertainties into account. The error bars are mainly due to measuring the faint [N II]λ6584 line.

2.4. Star formation rate and stellar mass

We derive the SFR from the Hα flux measured in the integrated spectrum of the galaxies following the Kennicutt (1998) relation. This SFR is also corrected for interstellar gas extinction. For each galaxy, the value of this extinction is an output of the SED fitting performed on extensive multi-band photometry (Contini et al. 2012). The method used to compute the SFR, the extinction-corrected SFR, and their associated errors is explained in Epinat et al. (2009). The median value of the errors on the SFR is 2.2 $M_\odot$ yr^{-1}.

The stellar masses, which are also an output of the SED-fitting procedure are those listed in Contini et al. (2012). Values of SFR (before and after extinction correction) and stellar masses are listed in Table 1.

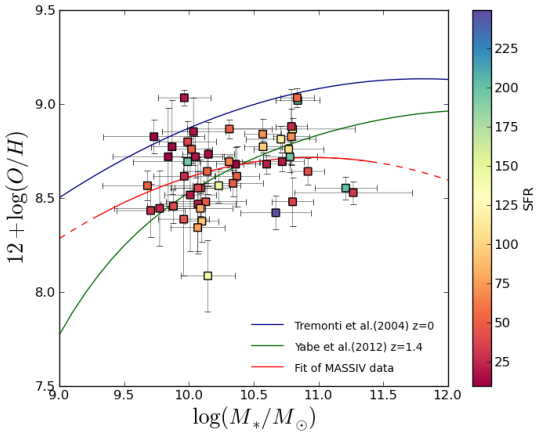

Fig. 3. Mass-metallicity relation. MASSIV galaxies are represented by coloured squares. The colour of the square scales with the value of the SFR. The red line is the best fit to the MASSIV sample. The mass-metallicity relations in the local universe (blue line) and at $z \sim 1.4$ (green line) are shown for comparison. Metallicities are given in the Tremonti et al. (2004) calibration.

Stellar masses and SFR have been computed using a Salpeter (1955) initial mass function (IMF). For the sake of consistency and to allow comparison with previous studies, stellar masses and SFR for other datasets computed with a different IMF have been corrected according to the offsets given in Bernardi et al. (2010). For instance, the relations from Tremonti et al. (2004), Yabe et al. (2012), and Lara-López et al. (2010) using Kroupa (2002) IMF have been shifted in Figs. 3–10, and 11. The relation of Mannucci et al. (2010) and stellar masses from Pérez-Montero et al. (2013) using Chabrier (2003) IMF have been corrected in Figs. 7, 8, and 12.

3. The mass-metallicity relation

Tremonti et al. (2004) give an expression of the relation between stellar mass and metallicity for a large sample of star-forming galaxies in the local universe:

$$Z = -0.08026m^2 + 1.847m - 1.492 \quad (2)$$

where $m = \log(M_*/M_\odot)$ and $Z = 12 + \log(\mathrm{O/H})$. The understanding of the shape of this relation is crucial to constraining the role of the various physical processes involved in galaxy evolution, such as outflows and gas accretion. It is also interesting to understand the causes for the metallicity dispersion around the median relation. Indeed, for a given stellar mass, a galaxy can have different gas-to-star mass ratios, SFR, or merger histories. These parameters influence the value of the metallicity and can explain the dispersion of the galaxies around the relation found by Tremonti et al. (2004). At high redshifts ($z > 3$), star-forming galaxies seem to follow a similar relation but at lower metallicity (Maiolino et al. 2008).

With the MASSIV sample, we can put constraints on the mass-metallicity relation in the redshift range $z \sim 0.9-1.8$. This relation can be compared with the one derived by Yabe et al. (2012) at redshift $z \sim 1.4$. To compute the metallicities, Yabe et al. (2012) used the Pettini & Pagel (2004) calibration of the N2 parameter. To have a better comparison with our data (see Fig. 3), we converted their metallicities into the Tremonti et al. (2004) calibration with the relation given in Kewley & Ellison (2008):

$$y = -738.1193 + 258.9673x - 30.05705x^2 + 1.167937x^3 \quad (3)$$

where x is the metallicity in Pettini & Pagel (2004) calibration and y the metallicity in the Tremonti et al. (2004) calibration.

Figure 3 shows that MASSIV galaxies are distributed around the Yabe et al. (2012) mass-metallicity relation. The best fit of MASSIV galaxies, resulting in a scattering of 0.2 dex, with a second-order polynomial relation has the following expression:

$$Z = -0.11m^2 + 2.45m - 4.71 \quad (4)$$

where $m = \log(M_*/M_\odot)$ and $Z = 12 + \log(\mathrm{O/H})$. This fit has a χ^2 of 0.850 and has been performed with the method of the least square the errors on both metallicity and mass taking into account. The agreement with either the Yabe et al. (2012) relation ($\chi^2 = 0.678$) or the Tremonti et al. (2004) relation offset to lower metallicities ($\chi^2 = 0.575$) is slighty worse.

Table 2. Median values of stellar mass and metallicity for the MASSIV sample separated in bins of mass and in bins of metallicity.

Stellar mass range	M_{median}	Z_{median}
$\log(M_*/M_\odot) \leq 10.00$	$9.87^{+0.11}_{-0.19}$	$8.62^{+0.38}_{-0.27}$
$10.00 < \log(M_*/M_\odot) \leq 10.15$	$10.07^{+0.08}_{-0.06}$	$8.52^{+0.33}_{-0.43}$
$10.15 < \log(M_*/M_\odot) \leq 10.70$	$10.36^{+0.30}_{-0.13}$	$8.68^{+0.91}_{-0.26}$
$\log(M_*/M_\odot) \geq 10.70$	$10.8^{+0.47}_{-0.09}$	$8.76^{+0.27}_{-0.28}$
Metallicity range	M_{median}	Z_{median}
$Z \leq 8.49$	$10.08^{+0.72}_{-0.37}$	$8.44^{+0.04}_{-0.35}$
$8.49 < Z \leq 8.65$	$10.19^{+1.08}_{-0.51}$	$8.57^{+0.08}_{-0.05}$
$8.65 < Z \leq 8.81$	$10.23^{+0.55}_{-0.39}$	$8.72^{+0.08}_{-0.04}$
$Z \geq 8.81$	$10.71^{+0.13}_{-0.98}$	$8.87^{+0.16}_{-0.06}$

3.1. Median values

The scatter around the mass-metallicity relation of MASSIV galaxies is quite important. It is thus interesting to compute the median value of metallicity and mass for different bins of stellar mass and bins of metallicity. We estimate the median value of metallicities and masses for four bins of mass and four bins of metallicity chosen to contain about the same number of galaxies in each bin. The median values are listed in Table 2. Figure 4 shows the median values of the metallicity for a binning in mass and the median values of the stellar mass for a binning in metallicity. These two sets of median values show that the mass-metallicity relation for the MASSIV sample is in good agreement with the Yabe et al. (2012) relation.

The relatively high value of the median metallicity for the lowest mass bin is certainly due to incompleteness in this mass range. Indeed, the metallicity was computed for 55% of the MASSIV galaxies in this mass bin, whereas metallicity was derived for more than 80% in higher mass bins. The median metallicity for $\log(M_*/M_\odot) \leq 10$ galaxies should thus be interpreted as an upper limit because low-metallicity galaxies in this low-mass range are difficult to probe owing to the faintness of the [N II]λ6584 emission line.

The median value of metallicity for the highest mass bin seems to be off the MZR fitted on the full sample (red line)

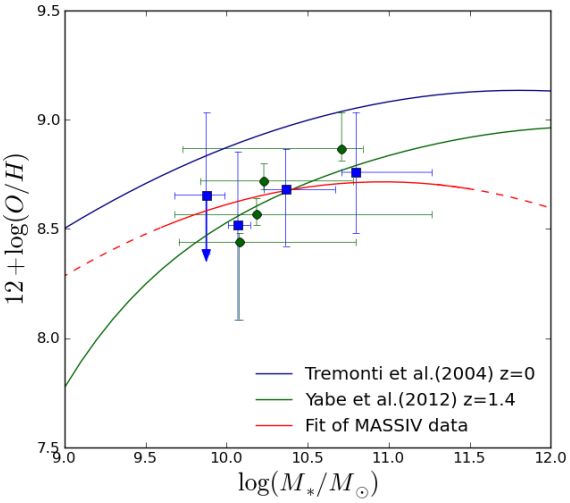

Fig. 4. Mass-metallicity relation with median values of stellar mass and metallicity for the MASSIV sample for a binning in mass (blue squares) and for a binning in metallicity (green dots). Error bars represent the dispersion around the median values. The arrow downward indicates that the median value of the metallicity for the lowest mass bin is certainly an upper limit due to incompleteness. Curves are the same as in Fig. 3.

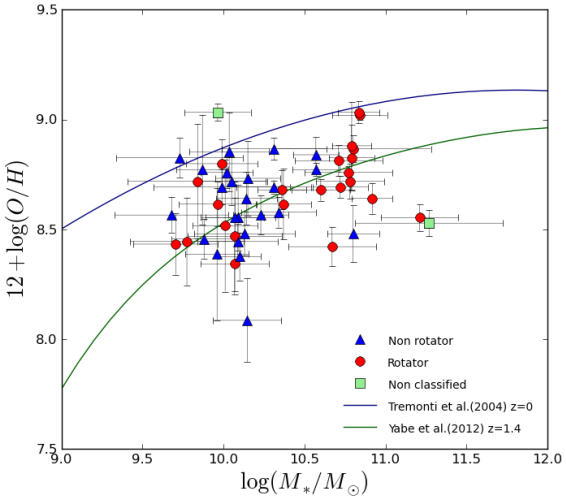

Fig. 5. Mass-metallicity relation for rotating (red dots) and non-rotating (blue triangles) MASSIV galaxies. The non-classified galaxies are shown as green squares. Curves are the same as in Fig. 3.

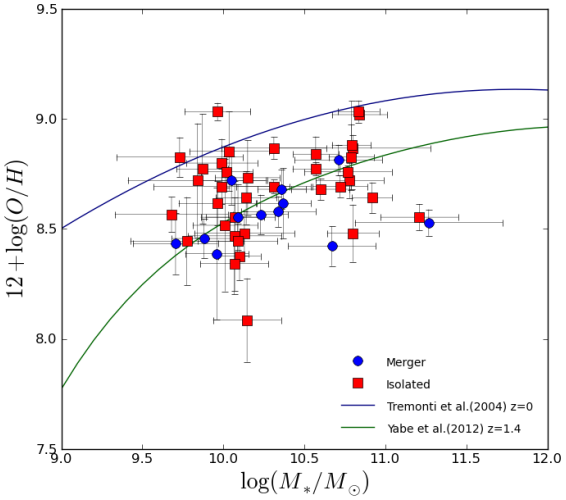

Fig. 6. Mass-metallicity relation for interacting (blue dots) and isolated (red squares) MASSIV galaxies. See Fig. 3 for lines description.

because, at high mass, this fit is dominated by two massive galaxies with fairly low metallicity. However the trend toward lower metallicities for the high mass end of the MZR is also present when combining the MASSIV galaxies with the *z*COSMOS sample (see Sect. 4.1 and Fig. 12).

3.2. Is there a link with kinematics and/or galaxy interactions?

Thanks to SINFONI IFU observations, a first-order kinematics classification of MASSIV galaxies was performed by Epinat et al. (2012) and Epinat et al. (in prep.). The galaxies with a velocity map showing clear velocity gradients are classified as rotating disks, whereas the other ones are classified as non-rotators. Figure 5 shows that there is no significant difference in the mass-metallicity relation between the two samples. The rotators have a median metallicity of 8.68 ± 0.19 with a median mass of 10.09 ± 0.11 and non-rotators of 8.64 ± 0.19 with a median mass of 10.64 ± 0.18. The main difference between the two samples is that the median mass of the rotators is higher than the median mass of non-rotators and almost all the galaxies with masses greater than $10^{10.5} M_\odot$ are rotators.

The metallicty of a galaxy could be affected by its close environment (e.g. Michel-Dansac et al. 2008). An accurate classification of the level of gravitational interaction of MASSIV galaxies is given in López-Sanjuan et al. (2013). Galaxies are classified in two main groups: interacting galaxies (major or minor mergers) and isolated galaxies. Figure 6 shows clearly that interacting galaxies in the MASSIV sample have lower metallicities (with a median value of 8.56 ± 0.12 and a median mass of 10.28 ± 0.17) than isolated galaxies which have a median value of metallicity of 8.69 ± 0.20 and a median mass of 10.14 ± 0.16.

4. Relations between stellar mass, metallicity, and SFR

Mannucci et al. (2010) propose a more fundamental relation between the stellar mass, SFR, and metallicity of star-forming galaxies in the local universe, a relation called fundamental metallicity relation (FMR). This relation does not seem to evolve with redshift at least up to $z \sim 2.5$. To visualize this relationship more easily, they propose a projection that removes the secondary dependences:

$$\mu_\alpha = \log(M_*/M_\odot) - \alpha \log(SFR). \quad (5)$$

Mannucci et al. (2010) find a value of $\alpha = 0.32$ that minimizes the scattering of galaxies around the FMR in the local universe, with a small residual dispersion of ∼0.05 dex in metallicity, i.e. ∼12 per cent. Figure 7 shows the FMR, i.e. the metallicity as a function of $\mu_{0.32}$, for the MASSIV sample. The metallicity has been (re)computed with the Tremonti et al. (2004) calibration as explained in Sect. 2.3, as well as the FMR from Mannucci et al. (2010) to account for different IMF (see Sect. 2.4). The intrinsic scatter of MASSIV galaxies around this relation is about 0.20 dex.

Figure 8 shows the FMR for MASSIV interacting and isolated galaxies. As for the mass-metallicity relation, there

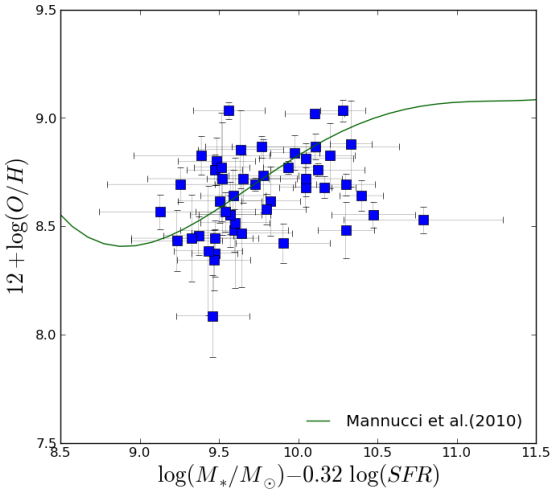

Fig. 7. Fundamental metallicity relation for MASSIV galaxies (blue squares) and assuming $\alpha = 0.32$ in Eq. (5). The FMR defined by Mannucci et al. (2010) for the star-forming galaxies in the local universe is shown as the green curve.

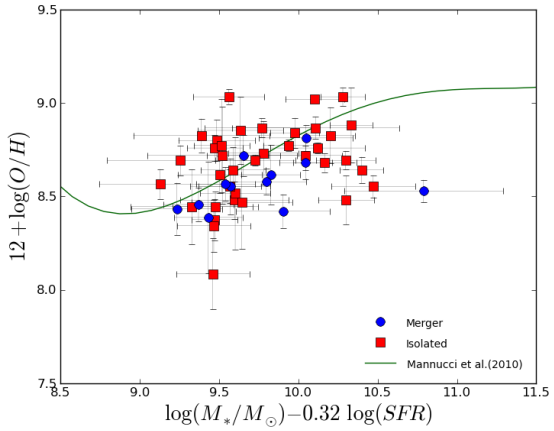

Fig. 8. Fundamental metallicity relation for MASSIV interacting (blue dots) and isolated (red squares) galaxies assuming $\alpha = 0.32$ in Eq. (5).

seems to be a significant difference between interacting and isolated galaxies. The intrinsic scattering around the FMR is about 0.12 dex for interacting galaxies and 0.20 dex for isolated ones. However, this difference could be due to the different sizes of the two sub-samples. To test this effect, we randomly pick 12 isolated galaxies among the 37 isolated ones of the MASSIV sample. This trial is repeated 1000 times in order to compute the scattering of these smaller samples, with a size similar to the interacting sample. The resulting median value of the scatter of these 1000 smaller samples is 0.18 dex, a value similar to the one measured in the observed sample of 37 isolated galaxies (see distribution in Fig. 9). We thus conclude that the difference of scattering between isolated and interacting MASSIV galaxies is significant. As for the mass-metallicity relation, we do not find any difference between rotating disks and non-rotators.

Lara-López et al. (2010) also studied the fundamental plane for star-forming galaxies of the local universe using the SDSS sample. They propose a projection where the stellar mass is fixed. This approach is motivated by the fact that the stellar mass is the most fundamental parameter of galaxies, with an evolution time scale longer than the SFR and metallicity. They thus defined a combination of the two other parameters (metallicity

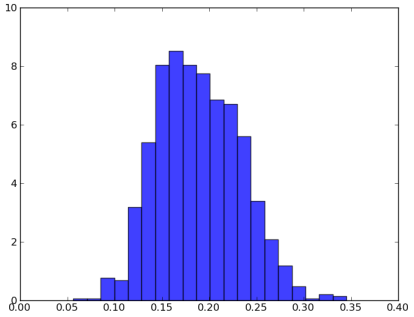

Fig. 9. Distribution of the scatter around the FMR for 12 isolated galaxies chosen randomly among the 37 isolated galaxies of the MASSIV sample.

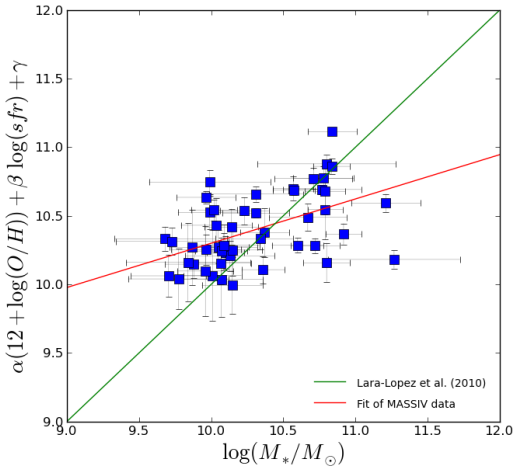

Fig. 10. Fundamental metallicity relation as defined by Lara-López et al. (2010), see Eq. (6). MASSIV galaxies are the blue squares.

and SFR) as

$$\log(M_*/M_\odot) = \alpha[12 + \log(\mathrm{O/H})] + \beta\log(SFR) + \gamma. \quad (6)$$

Lara-López et al. (2010) find a parametrization that minimizes the scattering around this relation at 0.16 dex when $\alpha = 1.122 \pm 0.008$, $\beta = 0.474 \pm 0.004$, and $\gamma = -0.097 \pm 0.077$. In their most recent paper, Lara-López et al. (2013) find other values for these parameters: $\alpha = 1.3764 \pm 0.006$, $\beta = 0.6073 \pm 0.002$, and $\gamma = -2.5499 \pm 0.058$. This new study includes galaxies up to redshift 0.36 from the GAlaxy and Mass Assembly (GAMA) survey, in addition to the data from the SDSS-DR7 already studied in their previous paper (Lara-López et al. 2010).

Figure 10 shows this relation for the MASSIV sample. We find *an intrinsic* scatter of 0.26 dex around the relation from Lara-López et al. (2010), which is slightly larger than the one we found with the FMR relation of Mannucci et al. (2010). However, our data do not follow the relation given by these values of α, β, and γ. MASSIV data are better fitted with the following relation:

$$\alpha[12 + \log(\mathrm{O/H})] + \beta\log(SFR) + \gamma = 0.323\log(M_*/M_\odot) + 7.071. \quad (7)$$

To derive these values, we performed a linear regression using least square method weighted on the errors of the three parameters.

We thus tried to minimize the *intrinsic* scattering of the MASSIV data around a relation with the same shape as proposed

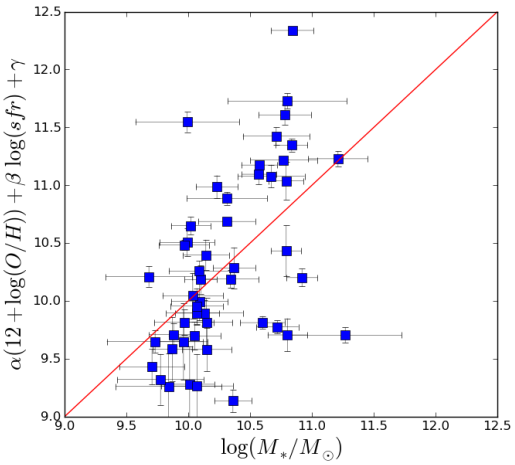

Fig. 11. Fundamental metallicity relation (red line) as defined by Lara-López et al. (2010) and fitted to the MASSIV data in order to minimize the scatter.

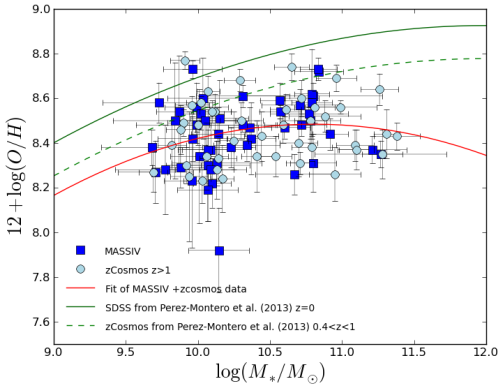

Fig. 12. Mass-metallicity relation. MASSIV galaxies are represented by blue squares. zCOSMOS galaxies are represented by light blue circles. The red line is the best fit to the MASSIV and zCosmos sample. The mass-metallicity relations in the local universe (green line) and at $0.4 < z < 1$ (green dashed line) are shown for comparison. Metallicities are given in the Pérez-Montero & Contini (2009) calibration.

by Lara-López et al. (2010) and found the following values for the parameters: $\alpha = 2.402$, $\beta = 1.811$, and $\gamma = -22.675$. These values of the parameters give a scatter of 0.15 dex which is lower than the scattering obtained with the other relations (see Fig. 11).

4.1. Comparison with zCOSMOS 20k sample

As shown previously, there is no convincing evidence that MASSIV galaxies do follow, with a reasonable small scatter, the so-called "fundamental" metallicity relations as defined by Mannucci et al. (2010) and Lara-López et al. (2010). To check whether there is any bias in the MASSIV sample, we can compare our dataset with another sample at similar redshift. Pérez-Montero et al. (2013) performed an exhaustive study of the redshift evolution of the mass-metallicity relation for a large sample of star-forming galaxies in the local and intermediate-redshift Universe ($z = 0.02-1.32$) from the SDSS and zCOSMOS-20k datasets. This sample contains more than 40 galaxies at $1 < z < 1.32$ that can be compared to the MASSIV sample.

Figure 12 shows clearly that there is no significant difference between the location of the two samples in the mass-metallicity plane. Corrections have been applied to the zCOSMOS sample in order to comply with the metallicity calibration and IMF used for the MASSIV sample. We thus fit the MASSIV data combined with the 43 galaxies from zCOSMOS. We found a fit similar to the one derived for the MASSIV sample alone. An evolution of the mass-metallicity relation with redshift is clearly seen in Fig. 12. Selection effects and incompleteness for the MASSIV sample are discussed in Sect. 3.1. The zCOSMOS sample has the same minimal selection as the VVDS sample (parent sample for MASSIV), i.e. a lower limit in apparent magnitude combined with a flux-limited selection of star-forming galaxies. The main difference between MASSIV and zCOSMOS is, however, the method (or emission lines) used to compute metallicity. It is based on the [N II]/Hα ratio for MASSIV galaxies but makes use of [O II]λ3727 and [Ne III]λ3869 emission lines for the zCOSMOS galaxies at $1 < z < 1.32$. Figure 12 shows clearly that there is no systematic difference in the metallicity estimates between the two samples even though they are derived with different methods/proxies. The two samples put together thus constitute a sample large enough to be considered as statistically significant.

Since it is known that metallicity is lower for higher SFR and that the mean SFR is higher at higher redshift at a given stellar mass, Pérez-Montero et al. (2013) also investigate whether this can be the cause of the observed evolution of the MZR. The relation between the SFR-corrected metallicity, using Eq. (8) of Pérez-Montero et al. (2013), and stellar mass for the combined MASSIV and zCOSMOS samples is very similar to the original mass-metallicity relation keeping a clear evolution with redshift.

This means that this evolution is not due to any SFR-based selection effect because it is still there when correcting the metallicity by the SFR. To investigate further that the evolution is really due to the redshift and not to selection effects that can occur when we compare galaxy samples at different redshifts or with different selection criteria, it is interesting to look at the relation between the stellar mass and the nitrogen-to-oxygen abundance ratio, also called MNOR. If the MNOR shows the same evolution with redshift as the MZR, it could mean that the evolution is real and that the FMR is not very fundamental, because the MNOR does not depend on SFR. Otherwise it could mean that the evolution we see is an artefact of the metallicity computation. Computing the nitrogen-to-oxygen abundance ratio for high-z individual galaxies is not an easy task since it requires detecting several emission lines for each galaxies. For the MASSIV sample we computed the nitrogen-to-oxygen abundance ratio from the nitrogen-to-sulphur line ratio as explained in Pérez-Montero & Contini (2009):

$$\log(\mathrm{N/O}) = 1.26\mathrm{N2S2} - 0.86 \quad (8)$$

where N2S2 is the ratio between the flux of [N II]$\lambda\lambda$6548, 6584 and [S II]$\lambda\lambda$6717, 6731. Considering the low S/N of the integrated spectra of MASSIV galaxies we were not able to measure the [S II]$\lambda\lambda$6717, 6731 doublet for the majority of galaxies. We thus used stacked spectra for two bins of stellar mass and measured the flux of [N II]$\lambda\lambda$6548, 6584 and [S II]$\lambda\lambda$6717, 6731 as described in Contini et al. (2012). We find a value of $\log(\mathrm{N/O}) = -0.74 \pm 0.25$ for $9.2 < \log(M_*/M_\odot) < 10.2$ and $\log(\mathrm{N/O}) = -0.88 \pm 0.30$ for $10.2 < \log(M_*/M_\odot) < 11.2$. We did not find any significant evolution of the MNOR between $z = 0$ (Pérez-Montero et al. 2013) and the one we tentatively derived at $z \sim 1.3$ with MASSIV stacked spectra. But with only two points at high redshift, it is hard to reach any firm conclusion.

5. Discussion and conclusions

In this paper we looked at some relations between fundamental parameters of 48 star-forming galaxies at $1 < z < 2$ for which we have been able to compute the metallicity from SINFONI data. First, we investigated the relation between stellar mass and metallicity in order to quantify its evolution with redshift. As expected and in agreement with previous studies (Queyrel et al. 2009), MASSIV galaxies are in good agreement with the mass-metallicity relation defined by Yabe et al. (2012) for galaxies at the same median redshift ($z \sim 1.3$) and the same ranges of stellar mass and SFR. This relation seems, however, to depend on the range of SFR we look at. We also found that the median value of metallicity and the scattering around this relation is slightly different for isolated and interacting galaxies. Interacting galaxies on average have lower metallicity than isolated ones, as also observed in the local universe (Michel-Dansac et al. 2008), and a lower dispersion around the MZR. It points to the importance of interactions in the chemical evolution of galaxies, but it can also be partially explained by the difference in mass range for the two samples.

We then investigated the relations involving stellar mass, metallicity, and SFR as done by Mannucci et al. (2010) and Lara-López et al. (2010). Indeed, these authors studied relations between these three parameters and find a fundamental plane that can be explained by an equilibrium model, such as the one developed by Finlator & Davé (2008), in which metallicity and SFR are strongly linked and mainly depend on gas inflows and outflows. Studies like the ones performed by Lara-López et al. (2010) and Mannucci et al. (2010) are observational studies that give empirical relations. The origin, and even the existence, of such relations are still being debated.

On one hand, models predict that if galaxies are in a stable situation, described by simple instantaneous recycling models, the stellar mass and metallicity should not depend on the SFR. Some recent studies, such as Sanchez et al. (2013) based on the CALIFA survey, find that metallicity does not depend on the SFR for a given mass range. They claim that the relations found by Lara-López et al. (2010) and Mannucci et al. (2010) may be biased by the way SFR are computed and the apertures used in the SDSS, hence by a selection effect depending on the redshift range studied. Nevertheless, in their recent paper, Lara-López et al. (2013) selected their sample taking this possible bias into account, and they imposed a low-redshift limit depending on the fibre diameter of the instrument used for the observations. Despite this restricted selection, they find a fundamental plan in their data with slightly different parameters.

On the other hand, a recent theoretical work has been performed (Lilly et al. 2013) deriving an equation relating mass, metallicity, and SFR from basic continuity equations, and it finds that SFR naturally appears as a second parameter in the mass-metallicity relation. Their equation gives a simple explanation of the fundamental metallicity relation and explains its independence with cosmic time. Other studies have been performed at higher redshift, such as Belli et al. (2013), and seem to confirm the existence of the fundamental relation but also its invariance with redshift, but the samples used for such analyses are often small compared to samples in the local universe, as for the MASSIV sample.

To investigate further and check for any possible bias, we compared the MASSIV dataset to *z*COSMOS galaxies at similar redshifts (Pérez-Montero et al. 2013). The MZR for the two samples are consistent and follow the expected relation for star-forming galaxies in the redshift range $z \sim 1-2$. In a second step we corrected the MZR by a function that depends on the SFR to remove the possible SFR-based selection effects, as performed in Pérez-Montero et al. (2013). We still observe an evolution with redshift, meaning that there should be also an evolution with redshift of the FMR.

To conclude, the relations we found in our study could be consistent with the analysis of Lara-López et al. (2010) and Mannucci et al. (2010) (if there is an evolution with redshift of their parameters), but given the size of our sample and the errors on the parameters, it is difficult to confirm strictly the lack of evolution of the FMR with redshift.

Acknowledgements. We thank N. Bouché and L. Michel-Dansac for useful discussions that helped improve this paper. We are grateful to the referee for useful comments. This work has been partially supported by the CNRS-INSU and its Programme National Cosmologie-Galaxies (France) and by the French ANR grant ANR-07-JCJC-0009. E.P.M. acknowledges the project AYA2010-21887-C04-01 of Spanish Plan for Astronomy and Astrophysics.

References

Belli, S., Jones, T., Ellis, R. S., & Richard, J. 2013, ApJ, 772, 141
Bernardi, M., Shankar, F., Hyde, J. B., et al. 2010, MNRAS, 404, 2087
Calura, F., Gibson, B. K., Michel-Dansac, L., et al. 2012, MNRAS, 427, 1401
Chabrier, G. 2003, ApJ, 586, L133
Contini, T., Garilli, B., Le Fèvre, O., et al. 2012, A&A, 539, A91
Cresci, G., Mannucci, F., Maiolino, R., et al. 2010, Nature, 467, 811
Cresci, G., Mannucci, F., Sommariva, V., et al. 2012, MNRAS, 421, 262
Epinat, B., Contini, T., Le Fèvre, O., et al. 2009, A&A, 504, 789
Epinat, B., Tasca, L., Amram, P., et al. 2012, A&A, 539, A92
Erb, D. K., Shapley, A. E., Pettini, M., et al. 2006, ApJ, 644, 813
Finlator, K., & Davé, R. 2008, MNRAS, 385, 2181
Franzetti, P., Scodeggio, M., Garilli, B., et al. 2007, A&A, 465, 711
Kennicutt, Jr., R. C. 1998, ARA&A, 36, 189
Kewley, L. J., & Ellison, S. L. 2008, ApJ, 681, 1183
Kroupa, P. 2002, Science, 295, 82
Lamareille, F., Mouhcine, M., Contini, T., Lewis, I., & Maddox, S. 2004, MNRAS, 350, 396
Lamareille, F., Contini, T., Brinchmann, J., et al. 2006, A&A, 448, 907
Lamareille, F., Brinchmann, J., Contini, T., et al. 2009, A&A, 495, 53
Lara-López, M. A., Cepa, J., Bongiovanni, A., et al. 2010, A&A, 521, L53
Lara-López, M. A., Hopkins, A. M., López-Sánchez, A. R., et al. 2013, MNRAS, 434, 451
Le Fèvre, O., Cassata, P., Cucciati, O., et al. 2013, A&A, 559, A14
Lequeux, J., Peimbert, M., Rayo, J. F., Serrano, A., & Torres-Peimbert, S. 1979, A&A, 80, 155
Lilly, S. J., Carollo, C. M., Pipino, A., Renzini, A., & Peng, Y. 2013, ApJ, 772, 119
López-Sanjuan, C., Le Fèvre, O., Tasca, L. A. M., et al. 2013, A&A, 553, A78
Maiolino, R., Nagao, T., Grazian, A., et al. 2008, A&A, 488, 463
Mannucci, F., Cresci, G., Maiolino, R., et al. 2009, MNRAS, 398, 1915
Mannucci, F., Cresci, G., Maiolino, R., Marconi, A., & Gnerucci, A. 2010, MNRAS, 408, 2115
Michel-Dansac, L., Lambas, D. G., Alonso, M. S., & Tissera, P. 2008, MNRAS, 386, L82
Moster, B. P., Naab, T., & White, S. D. M. 2012, MNRAS, 321
Pérez-Montero, E., & Contini, T. 2009, MNRAS, 398, 949
Pérez-Montero, E., Contini, T., Lamareille, F., et al. 2009, A&A, 495, 73
Pérez-Montero, E., Contini, T., Lamareille, F., et al. 2013, A&A, 549, A25
Pettini, M., & Pagel, B. E. J. 2004, MNRAS, 348, L59
Queyrel, J., Contini, T., Pérez-Montero, E., et al. 2009, A&A, 506, 681
Queyrel, J., Contini, T., Kissler-Patig, M., et al. 2012, A&A, 539, A93
Salpeter, E. E. 1955, ApJ, 121, 161
Sanchez, S. F., Rosales-Ortega, F. F., Jungwiert, B., et al. 2013, A&A, 554, A58
Stinson, G. S., Brook, C., Macciò, A. V., et al. 2013, MNRAS, 428, 129
Tremonti, C. A., Heckman, T. M., Kauffmann, G., et al. 2004, ApJ, 613, 898
Vergani, D., Scodeggio, M., Pozzetti, L., et al. 2008, A&A, 487, 89
Vergani, D., Epinat, B., Contini, T., et al. 2012, A&A, 546, A118
Yabe, K., Ohta, K., Iwamuro, F., et al. 2012, PASJ, 64, 60

Pages 9 to 10 are available in the electronic edition of the journal at http://www.aanda.org

Table 1. Fundamental parameters of the MASSIV sample.

VVDS ID (1)	Redshift (2)	Flux(Hα) (3)	[N II]/Hα (4)	*SFR* (5)	SFR_c (6)	Z_{PMC09} (7)	Z_{T04} (8)	log (M_*) (9)
020106882	1.3980	14.4 ± 2.4	0.23 ± 0.07	13.3 ± 0.8	38.10 ± 2.24	8.56 ± 0.11	8.80 ± 0.11	9.99 ± 0.22
020116027	1.5259	15.6 ± 1.5	0.13 ± 0.06	14.7 ± 3.6	42.20 ± 1.62	8.37 ± 0.15	8.55 ± 0.15	10.09 ± 0.23
020147106	1.5174	39.5 ± 4.0	0.08 ± 0.03	54.3 ± 6.8	92.10 ± 1.62	8.22 ± 0.11	8.38 ± 0.11	10.10 ± 0.38
020164388	1.3532	24.4 ± 2.5	0.11 ± 0.03	21.1 ± 1.1	46.50 ± 1.86	8.31 ± 0.10	8.48 ± 0.10	10.13 ± 0.31
020193070	1.0273	6.8 ± 1.5	0.20 ± 0.10	3.0 ± 0.4	14.40 ± 1.58	8.51 ± 0.17	8.73 ± 0.17	10.15 ± 0.20
020214655	1.0369	24.2 ± 7.4	0.20 ± 0.04	10.6 ± 0.5	51.70 ± 2.51	8.53 ± 0.07	8.76 ± 0.07	10.02 ± 0.16
020218856	1.3096	8.1 ± 0.9	0.10 ± 0.04	6.3 ± 0.6	29.65 ± 0.57	8.27 ± 0.14	8.43 ± 0.14	9.70 ± 0.26
020255799	1.0352	5.4 ± 1.5	0.21 ± 0.15	2.6 ± 0.3	12.80 ± 2.34	8.54 ± 0.25	8.77 ± 0.25	9.87 ± 0.16
020261328	1.5291	9.0 ± 2.7	0.12 ± 0.11	11.2 ± 1.0	19.00 ± 3.71	8.34 ± 0.30	8.52 ± 0.30	10.01 ± 0.20
020283083	1.2809	13.5 ± 2.5	0.19 ± 0.06	10.3 ± 0.8	17.40 ± 2.34	8.50 ± 0.11	8.72 ± 0.11	10.05 ± 0.21
020283830	1.3949	11.1 ± 1.8	0.15 ± 0.07	10.3 ± 1.0	50.40 ± 1.62	8.42 ± 0.16	8.62 ± 0.16	10.37 ± 0.17
020363717	1.3335	38.5 ± 4.2	0.13 ± 0.03	31.5 ± 3.6	53.40 ± 2.04	8.38 ± 0.08	8.57 ± 0.08	9.68 ± 0.20
020370467	1.3330	15.9 ± 2.5	0.25 ± 0.06	14.6 ± 2.5	71.20 ± 1.38	8.59 ± 0.08	8.84 ± 0.08	10.57 ± 0.14
020386743	1.0465	18.6 ± 2.2	0.10 ± 0.03	8.1 ± 0.8	39.40 ± 3.24	8.29 ± 0.09	8.46 ± 0.09	9.88 ± 0.21
020461235	1.0351	8.7 ± 0.9	0.18 ± 0.04	3.3 ± 0.9	9.60 ± 1.99	8.47 ± 0.09	8.68 ± 0.09	10.36 ± 0.14
140083410	0.9426	45.5 ± 4.3	0.13 ± 0.02	16.8 ± 1.2	37.10 ± 4.17	8.37 ± 0.09	8.55 ± 0.09	10.07 ± 0.18
140123568	1.0016	6.6 ± 0.8	0.24 ± 0.06	2.4 ± 0.5	11.80 ± 2.34	8.58 ± 0.09	8.83 ± 0.09	9.73 ± 0.40
140137235	1.0444	9.2 ± 1.6	0.11 ± 0.20	4.4 ± 1.1	21.60 ± 3.71	8.30 ± 0.25	8.47 ± 0.25	10.07 ± 0.29
140217425	0.9758	118.1 ± 4.4	0.36 ± 0.03	41.0 ± 1.9	200.00 ± 1.51	8.72 ± 0.02	9.01 ± 0.02	10.84 ± 0.17
140258511	1.2421	49.2 ± 2.2	0.26 ± 0.05	30.0 ± 1.9	146.40 ± 3.02	8.61 ± 0.06	8.87 ± 0.06	10.80 ± 0.48
140262766	1.2813	10.6 ± 2.6	0.19 ± 0.15	10.0 ± 3.8	10.00 ± 4.79	8.50 ± 0.26	8.72 ± 0.26	9.84 ± 0.43
140545062	1.0401	27.5 ± 3.4	0.17 ± 0.03	13.4 ± 1.5	22.70 ± 1.44	8.47 ± 0.05	8.68 ± 0.05	10.60 ± 0.18
220014252	1.3097	51.9 ± 6.9	0.19 ± 0.05	40.5 ± 2.5	197.50 ± 2.63	8.50 ± 0.08	8.72 ± 0.08	10.78 ± 0.21
220015726	1.3091	54.4 ± 1.8	0.21 ± 0.02	37.0 ± 5.2	106.40 ± 1.44	8.53 ± 0.03	8.76 ± 0.03	10.77 ± 0.27
220376206	1.2440	73.5 ± 8.0	0.09 ± 0.03	51.2 ± 3.9	249.70 ± 2.45	8.26 ± 0.09	8.42 ± 0.09	10.67 ± 0.27
220386469	1.0240	16.5 ± 6.3	0.11 ± 0.04	7.5 ± 1.1	36.50 ± 1.41	8.31 ± 0.13	8.48 ± 0.13	10.80 ± 0.16
220397579	1.0367	71.9 ± 9.4	0.13 ± 0.03	29.4 ± 4.0	143.20 ± 3.24	8.38 ± 0.09	8.57 ± 0.09	10.23 ± 0.17
220544103	1.3970	50.8 ± 7.4	0.23 ± 0.05	52.2 ± 1.4	117.50 ± 2.57	8.57 ± 0.07	8.81 ± 0.07	10.71 ± 0.27
220544394	1.0077	29.8 ± 3.8	0.14 ± 0.03	10.3 ± 0.7	50.10 ± 2.40	8.39 ± 0.07	8.58 ± 0.07	10.34 ± 0.23
220576226	1.0217	30.2 ± 3.1	0.18 ± 0.01	13.6 ± 0.7	66.30 ± 2.75	8.48 ± 0.03	8.69 ± 0.03	10.31 ± 0.23
220578040	1.0461	20.2 ± 1.6	0.18 ± 0.02	9.4 ± 0.9	20.80 ± 1.62	8.48 ± 0.05	8.69 ± 0.05	10.72 ± 0.16
220584167	1.4637	64.6 ± 2.9	0.13 ± 0.02	68.6 ± 3.4	202.60 ± 1.78	8.37 ± 0.06	8.55 ± 0.06	11.21 ± 0.25
910163602	1.3263	15.9 ± 3.1	0.37 ± 0.05	11.9 ± 2.0	54.35 ± 2.04	8.73 ± 0.05	9.03 ± 0.05	10.83 ± 0.12
910186191	1.5399	35.4 ± 6.0	0.12 ± 0.02	39.1 ± 6.1	31.43 ± 6.10	8.35 ± 0.06	8.53 ± 0.06	11.27 ± 0.45
910193711	1.5523	33.0 ± 6.9	0.18 ± 0.04	40.6 ± 22.7	197.70 ± 2.04	8.48 ± 0.08	8.69 ± 0.08	9.99 ± 0.18
910207502	1.4656	9.3 ± 1.2	0.26 ± 0.04	10.3 ± 1.0	50.22 ± 1.03	8.61 ± 0.05	8.87 ± 0.05	10.31 ± 0.33
910224801	1.3201	10.7 ± 3.1	0.37 ± 0.05	8.8 ± 1.8	18.12 ± 1.77	8.73 ± 0.04	9.03 ± 0.04	9.96 ± 0.20
910238285	1.5405	7.7 ± 3.0	0.16 ± 0.03	14.6 ± 2.6	41.89 ± 2.63	8.44 ± 0.07	8.64 ± 0.07	10.92 ± 0.13
910250031	1.6609	28.4 ± 1.4	0.03 ± 0.02	48.6 ± 5.6	139.84 ± 5.58	7.92 ± 0.19	8.09 ± 0.19	10.15 ± 0.20
910259245	1.5174	4.9 ± 1.8	0.27 ± 0.15	5.6 ± 1.0	27.08 ± 0.98	8.62 ± 0.20	8.88 ± 0.20	10.79 ± 0.12
910261247	1.4262	18.8 ± 3.3	0.21 ± 0.02	19.8 ± 1.1	96.78 ± 1.14	8.54 ± 0.03	8.77 ± 0.03	10.57 ± 0.14

Notes. Column 1 lists the VVDS identification number. Column 2 gives the redshift. Columns 3 and 4 list the Hα flux (in erg s^{-1} cm^{-2}) and the flux ratio [N II]/Hα respectively. The star formation rate (in $M_\odot$ yr^{-1}) is given in Cols. 5 (not corrected for extinction) and 6 (dereddened value). Columns 7 and 8 list the metallicity computed with the Pérez-Montero & Contini (2009) and Tremonti et al. (2004) calibrations respectively. Stellar mass (in log of $M_\odot$) is given in Col. 9 (from Contini et al. 2012).

Table 1. continued.

VVDS ID (1)	Redshift (2)	Flux(Hα) (3)	[N II]/Hα (4)	SFR (5)	SFR_c (6)	Z_{PMC09} (7)	Z_{T04} (8)	log (M_*) (9)
910266034	1.5642	15.8 ± 4.0	0.08 ± 0.03	20.4 ± 3.0	76.25 ± 2.95	8.19 ± 0.14	8.34 ± 0.14	10.07 ± 0.20
910276733	1.3390	3.8 ± 0.9	0.16 ± 0.06	11.0 ± 2.1	53.67 ± 2.11	8.44 ± 0.12	8.64 ± 0.12	10.14 ± 0.19
910279515	1.3983	14.2 ± 1.5	0.24 ± 0.11	14.2 ± 2.0	69.00 ± 4.68	8.58 ± 0.15	8.83 ± 0.15	10.79 ± 0.14
910279755	1.3127	23.5 ± 1.4	0.15 ± 0.05	16.3 ± 1.3	27.71 ± 1.29	8.42 ± 0.10	8.62 ± 0.10	9.96 ± 0.24
910337228	1.3972	15.8 ± 1.2	0.09 ± 0.08	39.1 ± 16.6	44.97 ± 16.57	8.23 ± 0.30	8.39 ± 0.30	9.96 ± 0.20
910340496	1.3981	4.5 ± 0.6	0.26 ± 0.13	3.7 ± 0.5	17.95 ± 0.50	8.60 ± 0.18	8.85 ± 0.18	10.03 ± 0.25
910370574	1.6632	12.6 ± 1.5	0.10 ± 0.02	16.8 ± 3.6	82.00 ± 3.65	8.28 ± 0.08	8.44 ± 0.08	10.09 ± 0.24